Aerospace Science and Technology 168 (2026) 110856

Contents lists available at ScienceDirect

Aerospace Science and Technology

journal homepage: www.elsevier.com/locate/aescte

Original article

Lateral-directional trim for air and ground minimum control speeds evaluation in conceptual design

Gabriele Morra *, Claudio Mirabella, Fabrizio Nicolosi, Pierluigi Della Vecchia

University of Naples Federico II, Department of Industrial Engineering, Via Claudio, 21, Naples, 80125, Italy

ARTICLE INFO

Communicated by Christian Circi

Keywords:
Minimum control speed in air
Minimum control speed on ground
Simulated flight test
Conceptual aircraft design

ABSTRACT

This paper presents the development of a comprehensive methodology for accurately estimating minimum control speeds both in the air (V_{MCA}) and on the ground (V_{MCG}), addressing a gap in conceptual design methodologies. These speeds are critical for appropriately sizing the rudder and vertical tailplane and ensuring controllability during one-engine-inoperative scenarios. The proposed approach integrates a nonlinear lateral-directional trim analysis and a time-domain simulation of ground manoeuvres, accounting for landing gear-runway interaction effects. The methodology facilitates a precise and rapid estimation of V_{MCA} and V_{MCG} while adhering to physical and regulatory constraints, making it suitable for early design iterations. It serves as a key procedure for optimising the design of aircraft with Short Take Off and Landing capabilities, which may exhibit controllability issues at near-stall speeds. A comparison of the data with those documented in the C-130J *Performance Data Manual* and the ATR 72–500 *Flight Crew Operating Manual* exhibits a close match across a wide range of operational conditions.

1. Introduction

The Air Minimum Control Speed (V_{MCA}) and Ground Minimum Control Speed (V_{MCG}) are critical for ensuring aircraft controllability in the event of engine failure.

V_{MCA} represents the minimum speed at which an aircraft can maintain controlled, level flight after an engine failure. This parameter is particularly critical for Short Take-Off and Landing (STOL) aircraft, operating at low speeds and on limited runway lengths. It is imperative that V_{MCA} is determined with the utmost precision to avoid loss of control typically experienced during the initial airborne phase. Due to their high-lift configurations and low stall speeds, STOL aircraft require correspondingly low minimum control speeds to maintain safe handling characteristics and good overall performance.

Similarly, V_{MCG} represents the minimum speed at which the directional control can be maintained on the ground during takeoff. This parameter becomes particularly important for aircraft with high thrust-to-weight ratios operating on narrow runways. It directly affects the design of ground control systems and landing gear.

The reader should be aware of all the safety-related aspects when reading the following sections of this article. A considerable number of fatal accidents have been linked to failure to adhere to minimum control speed requirements, particularly under tactical or emergency operating conditions. Additionally, training scenarios that simulate emergencies, especially engine failures during check rides, have been identified as a significant source of accidents involving less-experienced pilots. One such case is detailed in the Australian Transport Safety Bureau (ATSB) report [1]. Further analyses of similar events can be found in [2]. Horlings [3] provides a comprehensive overview of the loss of control accidents resulting from aircraft operating below the minimum control speeds specified in official flight manuals.

The importance of V_{MCA} goes beyond safety; it directly influences the design of the vertical tailplane and crucial control surfaces such as the rudder, and also affects the actual operational capabilities of the aircraft. Recent studies focus on tailplane aerodynamic optimizations [4], but a conceptual design carried out with the presented approach is an excellent starting point for a viable configuration.

Given the critical role of V_{MCA} and V_{MCG} in the design and operational safety of an aircraft, there is a strategic need to develop reliable methodologies for its estimation during the conceptual design phase.

Regrettably, the existing literature provides limited guidance on the evaluation of these characteristic speeds during the early stages of aircraft design. Several authors, such as Sadraey [5] and Torenbeek [6, p. 336], suggest the use of statistical methodologies. Roskam [7, p. 26] remains the most valuable reference, as he addresses the problem of three-axis equilibrium. However, Roskam's methodology does not

* Coresponding author.
E-mail address: gabriele.morra@unina.it (G. Morra).

https://doi.org/10.1016/j.ast.2025.110856
Received 3 October 2024; Received in revised form 30 May 2025; Accepted 28 August 2025
Available online 3 September 2025

Nomenclature

α	Angle of attack referred to the x-body axes
$\dot{\psi}$	Heading rate
ψ	Heading angle
b_w	Wingspan
C_L	Aircraft lift coefficient
g_0	Standard gravitational acceleration
h	Above sea-level height
I_{zz}	Principal moment of Inertia along the z-body axes
M	Mach number
q	Dynamic pressure
S_w	Wing reference Surface
V_{MCA}	Minimum control speed in air
V_{MCG}	Minimum control speed on ground
W	Aircraft weight
w	Side-displacement
x_{mL}	Main Left landing gear
x_{mR}	Main Right landing gear
x_n	Nose landing gear
y_e	Critical engine yaw moment arm
AFM	Aircraft Flight Manual
CAS	Calibrated Airspeed
CS	Certification Specifications
FAR	Federal Aviation Rules
FCOM	Flight Crew Operating Manual
ISA	International Standard Atmosphere
STOL	Short Take Off and Landing

account for nonlinearities and differs from the approach proposed in this article in two key ways: it requires the selection of specific flight conditions (i.e., a given flight speed and bank angle) and a predetermined thrust setting (i.e., engine-induced moments along the aircraft's three control axes). The procedure implemented in this study appears to be more accurate and straightforward-thanks to the nonlinear solver-when compared with other approaches, such as the one proposed by Hadder and Takahashi [8].

In early design stages, vertical tailplanes are often sized with conservative margins to account for uncertainties and anticipated certification requirements. This study contributes to improving the accuracy of their sizing by incorporating regulatory considerations earlier in the process. Unlike traditional asynchronous approaches, where simplified methods are used initially and compliance is verified later, this methodology promotes a more integrated design workflow, thereby reducing technical risks and the likelihood of costly redesigns.

Given that current aircraft design practices often rely on simplified assumptions that may not adequately capture the complexity of modern configurations [9], there is a growing need for more rigorous methodologies to estimate these critical speeds. This study addresses a critical gap by introducing a comprehensive framework that explicitly accounts for nonlinear lateral-directional trim analysis and tyre-runway interaction modelling-factors that are often simplified or overlooked in early-stage design tools. By simulating engine-out manoeuvres and integrating these critical effects, the methodology enhances the accuracy and reliability of minimum control speed predictions from the earliest stages of the design process.

Section 2 outlines the regulatory framework governing aircraft control speed requirements, with an emphasis on implications for flight safety and certification. Section 3 presents the theoretical foundation and computational methodology developed for assessing minimum control speed constraints, detailing the nonlinear solution approach and its implementation. In Section 4, the results are presented and discussed through two representative applications, including a comparative benchmarking analysis against established methods. The concluding section synthesizes the key contributions of this work and explores the broader implications for aircraft conceptual design and certification processes.

2. Regulatory framework and control speed requirements

This section outlines the key regulatory elements that underpin the assessment of minimum control speeds, focusing on their relevance for aircraft design and certification. From a design perspective, these regulatory requirements impose clear constraints on aerodynamic performance, engine-out handling, and control authority.

Regulatory agencies such as the European Union Aviation Safety Agency (EASA) and the Federal Aviation Administration (FAA) enforce stringent requirements for the certification of large commercial aircraft [10,11]. Among these, particular emphasis is placed on minimum control speeds-both airborne and ground-based-which define the threshold below which directional control cannot be ensured following the sudden failure of a critical engine. These speeds are closely linked to the reference stall speed (V_{SR}) and are constrained by operational conditions involving asymmetric thrust, specific centre-of-gravity configuration, and flight control limitations.

According to the Aircraft Flight Manuals, the indicated V_{MCA} represents the *standardised* minimum control speed in air [12]. In this context, the sideslip angle β is assumed to be zero, reflecting coordinated flight conditions in which the aircraft maintains directional control within regulatory limits.

The methods presented in this study have been developed in strict accordance with applicable airworthiness standards and are designed to replicate the prescribed certification manoeuvres through simulation. This approach enables a preliminary assessment of compliance with CS or FAR regulations (as indicated by the validation errors discussed in Section 4), thereby supporting the robustness and safety of the conceptual design.

Additional technical details, including full regulatory definitions, test configurations, and procedural steps, are provided in Appendix A for reference.

3. Methodology

3.1. Minimum control speed in air

The calculation of the air minimum control speed begins with the lateral-directional trim equations. Specifically, the flight test is simu-

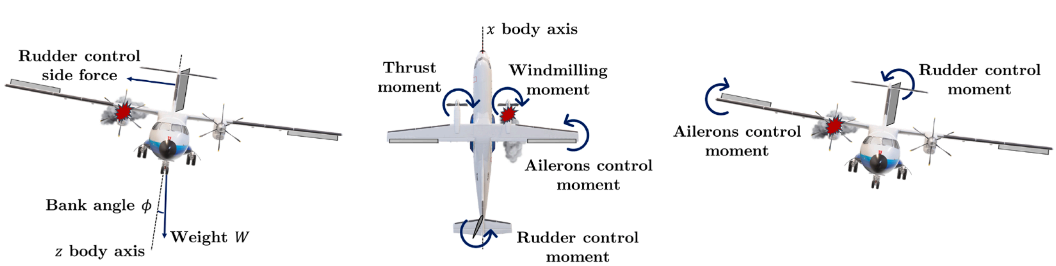

Fig. 1. Roll, yaw, and side-force free body diagrams for a twin-engine aircraft in OEI condition.

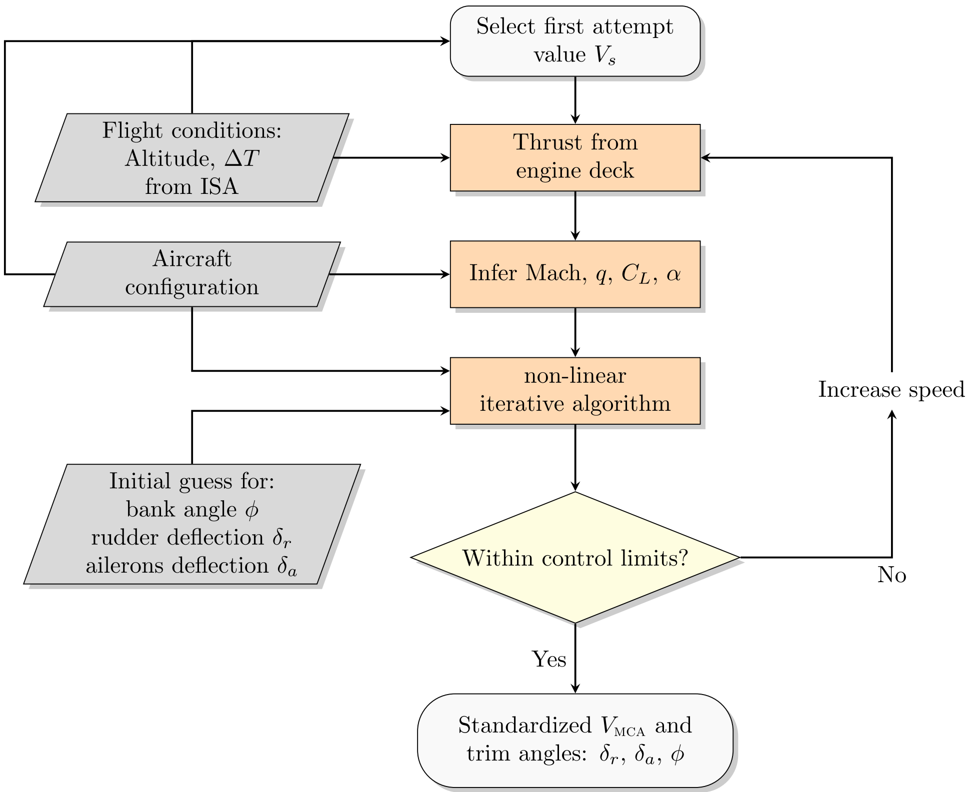

Fig. 2. Flowchart for standardised V_{MCA} and multi-axis trim computation.

lated by identifying the lowest speed at which the aircraft achieves a trim condition-an equilibrium state with no net side force, yawing moment, or rolling moment. The mathematical reference frame used for this analysis is derived from the free-body diagram shown in Fig. 1 and is described in detail below:

$$\begin{bmatrix} C_{\mathcal{N}_\beta} & C_{\mathcal{N}_{\delta_r}} & C_{\mathcal{N}_{\delta_a}} & 0 \\ C_{Y_\beta} & C_{Y_{\delta_r}} & C_{Y_{\delta_a}} & \dfrac{W}{q\,S_w} \\ C_{\mathcal{L}_\beta} & C_{\mathcal{L}_{\delta_r}} & C_{\mathcal{L}_{\delta_a}} & 0 \end{bmatrix} \begin{bmatrix} \beta \\ \delta_r \\ \delta_a \\ \sin(\phi) \end{bmatrix} = \begin{bmatrix} \dfrac{T\,y_e}{q\,S_w\,b_w} \\ 0 \\ 0 \end{bmatrix} \tag{1}$$

where

$C_{\mathcal{N}_\beta} = \dfrac{\partial C_{\mathcal{N}}}{\partial \beta}(M, h, \Delta_{ISA}, W)$ = Aircraft yaw stability derivative

$C_{Y_\beta} = \dfrac{\partial C_Y}{\partial \beta}(M, h, \Delta_{ISA}, W)$ = Sideslip-induced side-force derivative

$C_{\mathcal{L}_\beta} = \dfrac{\partial C_{\mathcal{L}}}{\partial \beta}(M, h, \Delta_{ISA}, W)$ = Sideslip-induced roll moment derivative

$C_{\mathcal{N}_{\delta_r}} = \dfrac{\partial C_{\mathcal{N}}}{\partial \delta_r}(\delta_r, M, h, \Delta_{ISA}, W)$ = Rudder control power derivative

$C_{Y_{\delta_r}} = \dfrac{\partial C_Y}{\partial \delta_r}(\delta_r, M, h, \Delta_{ISA}, W)$

= Lateral force due to rudder deflection

$C_{\mathcal{L}_{\delta_r}} = \dfrac{\partial C_{\mathcal{L}}}{\partial \delta_r}(\delta_r, M, h, \Delta_{ISA}, W)$

= Rudder-induced roll moment derivative

Table 1
Angles limitations imposed to simulate V_{MCA} for the C-130J.

Variable	Limitation	Rationale
Sideslip angle β	$\leq \lvert 10^\circ \rvert$	Avoid significant reduction in lateral-directional stability and excessive increment of drag.
Rudder deflection δ_r	$\leq \lvert 30^\circ \rvert$	Reached maximum control surface deflection and/or avoid control surface stall.
Ailerons deflection δ_a	$\leq \lvert 20^\circ \rvert$	Reached maximum control surface deflection and/or avoid control surface stall.
Bank angle ϕ	$\leq \lvert 5^\circ \rvert$	Regulatory prescription.

$C_{\mathcal{N}_{\delta_a}} = \dfrac{\partial C_{\mathcal{N}}}{\partial \delta_a}(\delta_a, M)$ = Ailerons adverse yaw effect

$C_{Y_{\delta_a}} = \dfrac{\partial C_Y}{\partial \delta_a}(\delta_a, M)$ = Lateral force due to ailerons deflection

$C_{\mathcal{L}_{\delta_a}} = \dfrac{\partial C_{\mathcal{L}}}{\partial \delta_a}(\delta_a, M)$ = Ailerons control power derivative

$T = T(M, h, \Delta_{ISA})$ = Single engine thrust

The system of equations is underdetermined, as the number of unknowns exceeds the number of available constraints, resulting in infinitely many possible solutions. Moreover, the problem is strongly nonlinear, since control derivatives depend on the unknown control surface deflections.

Physical constraints further restrict the solution space, as any configuration exceeding predefined limits must be discarded. Table 1 presents angular constraints which distinguish between feasible and non-feasible

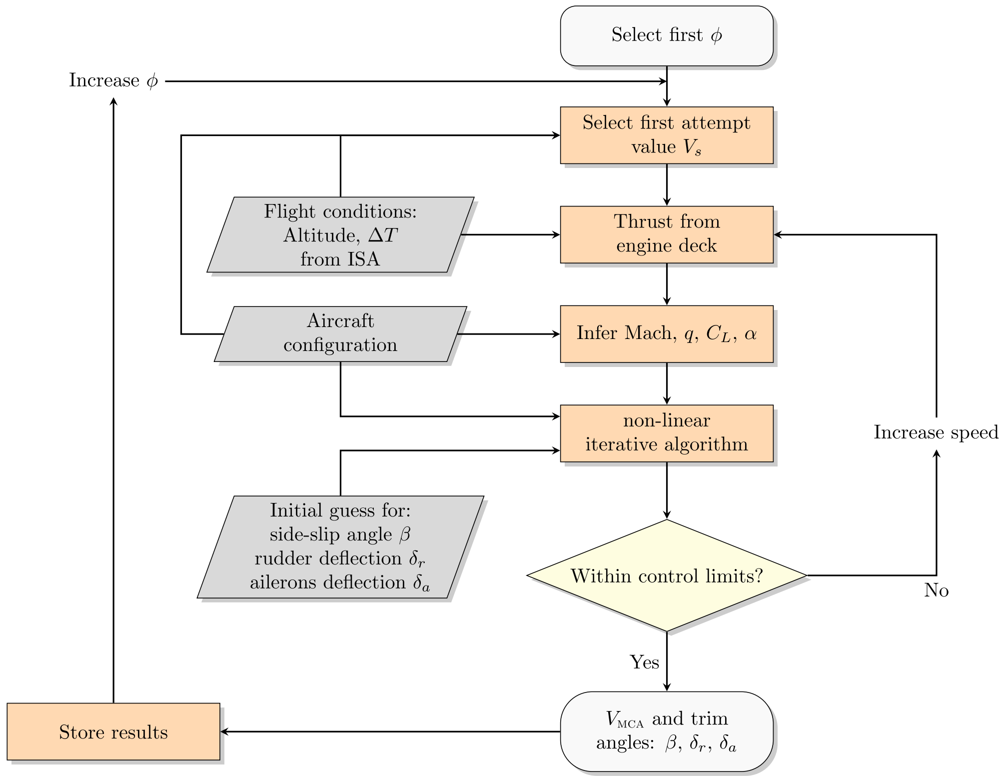

Fig. 3. Flowchart for ϕ-dependant V_{MCA} and multi-axis trim computation.

solutions. In this context, the rationale for imposing such constraints is grounded in practical considerations and supported by the guidelines proposed by Roskam [7]. These limitations are intended to prevent excessive control surface deflections and sideslip angles that could lead to surface stall, unacceptable increases in drag, or degradation of stability characteristics. Importantly, the applied constraints remain well within the aircraft-s operational envelope and are consistent with standard pilot best practices and established procedures.

A schematic representation of the computational algorithm is provided in Fig. 2. The V_{MCA} calculation routine begins with an initial guess, typically set to the stall speed-the minimum speed at which level flight can be sustained. Lateral-directional trim solutions are not computed for speeds below this threshold, as such conditions represent physically unrealistic and aerodynamically meaningless flight scenarios. Accordingly, this value defines the *stall-limited standardised* V_{MCA}.

This algorithm enables the calculation of both the stall-limited standardised V_{MCA} and the equilibrium angles required for lateral-directional trim: the bank angle ϕ, and the deflections of the rudder and ailerons δ_r and δ_a respectively. The following system of trim equations is derived from (1) with $\beta = 0$:

$$\begin{bmatrix} C_{\mathcal{N}_{\delta_r}} & C_{\mathcal{N}_{\delta_a}} & 0 \\ C_{Y_{\delta_r}} & C_{Y_{\delta_a}} & \dfrac{W}{q\,S_w} \\ C_{\mathcal{L}_{\delta_r}} & C_{\mathcal{L}_{\delta_a}} & 0 \end{bmatrix} \begin{bmatrix} \delta_r \\ \delta_a \\ \sin(\phi) \end{bmatrix} = \begin{bmatrix} \dfrac{T\,y_e}{q\,S_w\,b_w} \\ 0 \\ 0 \end{bmatrix} \tag{2}$$

The system (2) was solved using a well-established nonlinear algorithm [13,14].

To actively test the methodology and the physical results obtained, additional routines were developed to calculate V_{MCA} values across a range of aircraft weights and bank angles. These two variables are crucial for understanding how V_{MCA} varies depending on the aircraft's load configuration (weight) and the pilot's behaviour in low-speed scenarios, particularly in the event of an unexpected engine failure. Specifically, the routine illustrated in Fig. 3 computes how V_{MCA} changes with varying bank angles, which directly reflects the pilot's aileron inputs. This enables an analysis of how active control inputs may influence the aircraft-s controllability, offering valuable insights into pilot actions that could help maintain safety during flight.

The same method can be used to analyse how controllability varies with aircraft weight. This enables an assessment of the pilot-s required actions under different loading conditions. As detailed in Section 4, weight plays a critical role in controllability during one-engine-inoperative scenarios: it may either enhance or impair controllability, depending on the circumstances.

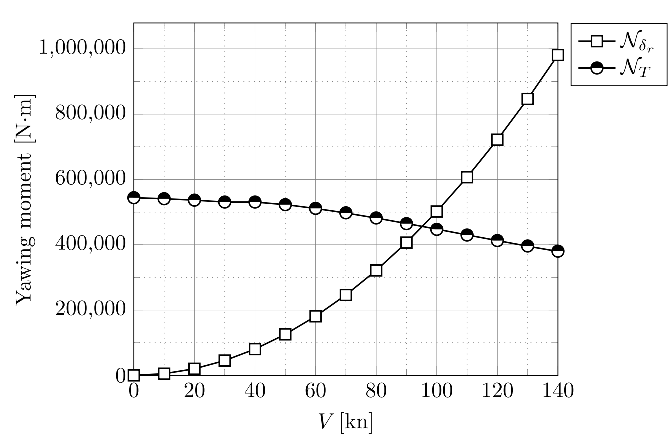

Fig. 4. Yawing moment due to critical engine failure $\mathcal{N}_T$ and rudder control moment $\mathcal{N}_{\delta r}$ for a simulated C-130J-30, where $\mathcal{N}_T$ and $\mathcal{N}_{\delta r}$ represent the magnitudes of the associated vectors.

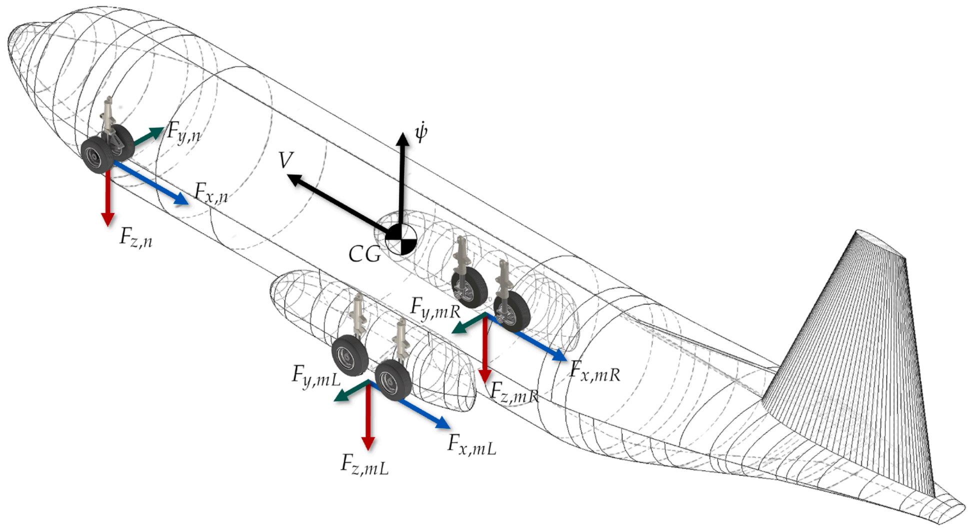

Fig. 5. Free-body diagram of a landing gear under a resultant negative yawing moment according to the European convention.

3.2. Minimum control speed on ground

A common method for estimating V_{MCG} involves calculating the yawing moment vectors produced by asymmetric thrust $\mathcal{N}_T$ and maximum rudder deflection $\mathcal{N}_{\delta_r}$. By examining these moments across a range of speeds (Fig. 4), the equilibrium condition $\mathcal{N}_T + \mathcal{N}_{\delta_r} = 0$ identifies the minimum speed at which the pilot can maintain directional control on the ground and counteract the yawing tendency.

However, this calculation does not account for the maximum lateral displacement permitted by regulations, as outlined in Section 2, and is therefore likely to overestimate V_{MCG}. While this procedure may serve as a first approximation for estimating V_{MCG}, it is not sufficiently reliable when addressing specific design considerations or when stringent requirements must be met. For tactical military, STOL aircraft, for example, the ability to operate under strict constraints-such as narrow or even semi-prepared runways-is often essential. Accordingly, this study builds on the observations above to conduct a manoeuvre-based simulation for estimating V_{MCG} in compliance with regulatory standards.

The manoeuvrer on the runway is simulated starting from a trial speed V_{ef}, which represents the speed at which the engine failure occurs. The evolution of the translational equations in the runway plane, along with the yawing moment induced by the OEI condition must then be analysed. The roll moment can be neglected as a first approximation, as it is counteracted by the damping effect of the landing gear. For this reason, aileron deflection is not considered significant in the simulation-although, in practice, the pilot would also use the ailerons to generate an alleviation drag moment [15].

To a good approximation, the aircraft can be considered a rigid body. By analysing the problem in a reference frame that is inertial with respect to the aircraft, it is therefore possible to apply Euler's laws of motion in this vector form:

$$\frac{W}{g_0}\dot{\boldsymbol{V}} = (N_{\text{engines}} - 1)\,\boldsymbol{T} + \boldsymbol{D}_{\text{aerodynamics}} + \boldsymbol{D}_{\text{windmilling}} + \boldsymbol{F}_{\text{landing gear}} \tag{3}$$

$$I_{zz}\,\ddot{\boldsymbol{\psi}} = \mathcal{N}_T + \mathcal{N}_{\delta_r} + \mathcal{N}_{\text{landing gear}} \tag{4}$$

Here, $\dot{\boldsymbol{V}}$ denotes the first derivative of the translational velocity $\boldsymbol{V}$ with respect to time, and $\ddot{\boldsymbol{\psi}}$ denotes the second derivative of the heading angle $\boldsymbol{\psi}$ with respect to time. The term N_{engines} represents the total number of aircraft engines. The vectors $\boldsymbol{D}_{\text{aerodynamics}}$ and $\boldsymbol{D}_{\text{windmilling}}$ correspond to the drag forces due to aerodynamic effects and windmilling propellers, respectively. Finally, $\boldsymbol{F}_{\text{landing gear}}$ and $\mathcal{N}_{\text{landing gear}}$ denote the frictional force and reaction moment resulting from the interaction between the tyres and the runway.

The calculation routine begins with a trial speed V_{ef} slightly lower than that determined by the intersection shown in Fig. 4, and simulates the temporal evolution of the aircraft's motion along the runway.

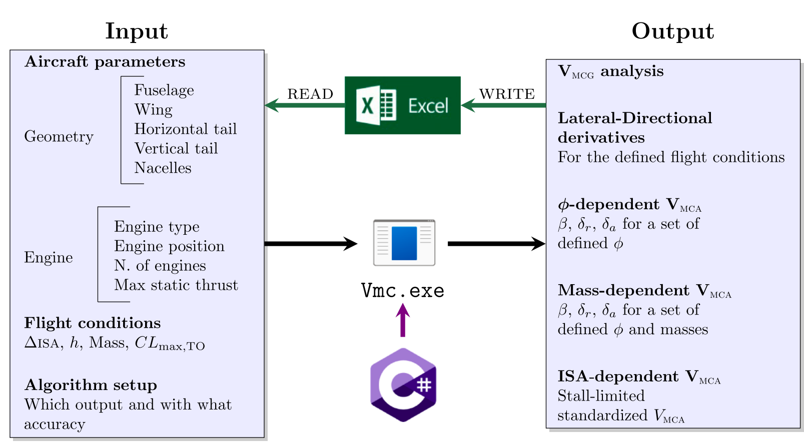

Fig. 6. Diagram of the calculation procedure that has been implemented.

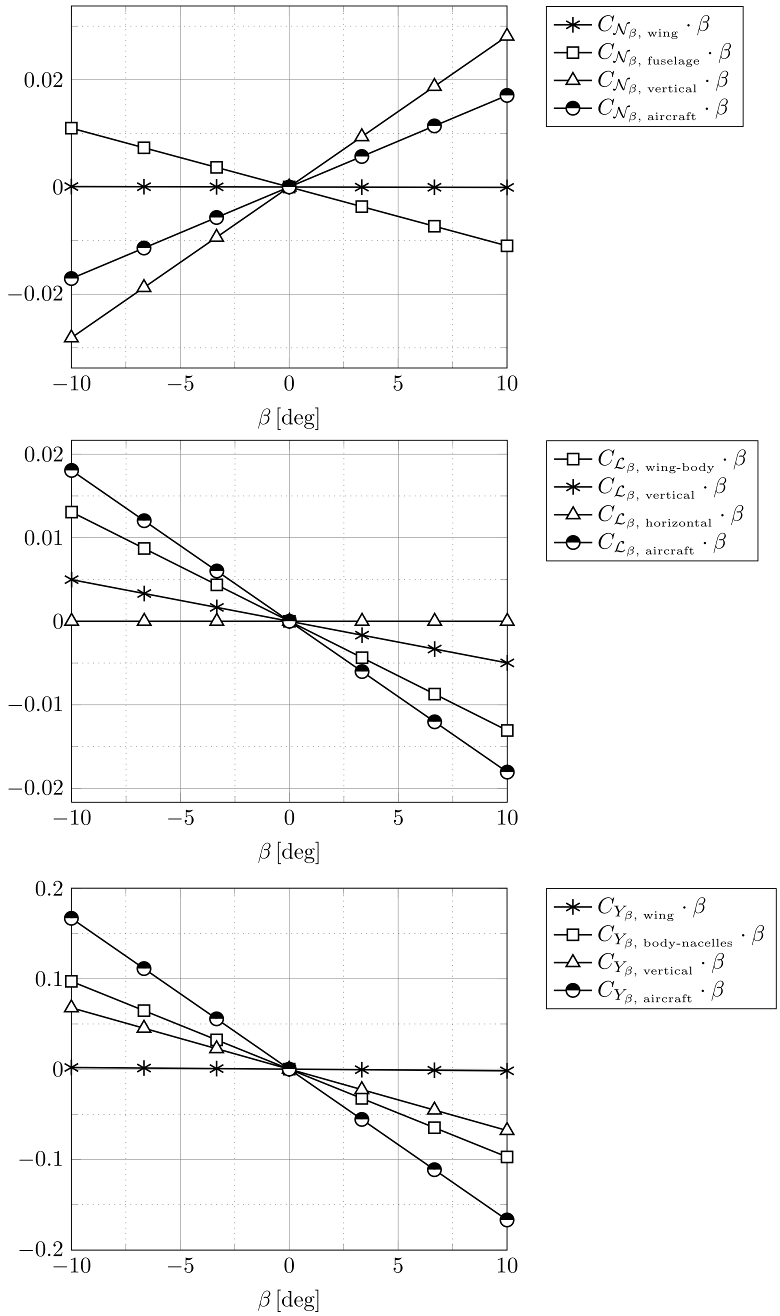

Fig. 7. Lateral-directional stability derivatives for a simulated C-130J-30 at Mach 0.2.

Through an iterative approach, it is possible to determine the precise value of V_{ef} that results in a lateral deviation of 9.1m (30 ft) from the runway centreline. By definition, this value of V_{ef} corresponds to the ground minimum control speed V_{MCG}. The calculation of V_{MCG} is highly sensitive to initial conditions. Therefore, during the conceptual design phase, it is advisable to refer to existing aircraft to establish accurate design parameters. A notable example is the moment of inertia I_{zz}. In this study, the first-level estimation procedure proposed by Roskam was employed [16] and it was deemed adequate for this analysis.

3.3. Landing gear-runway interaction

Accurate modelling of the interaction between the landing gear and the runway is of paramount importance. The vertical load distribution can be estimated based on the aircraft's geometry and landing gear configuration. Let x_m and x_n denote the distances from the centre of gravity (CG) to the main and nose landing gear, respectively. Under these definitions, the following relationship can be derived:

$$F_{z,n} = W \, \frac{x_m}{x_m + x_n} \tag{5}$$

$$F_{z,mL} = F_{z,mR} = \frac{1}{2} \, W \, \frac{x_n}{x_m + x_n} \tag{6}$$

The subscripts n, mL, and mR refer to the nose, main left, and main right landing gear, respectively. Furthermore, the frictional forces are considered as projected along the body axes, as shown in Fig. 5.

Starting from the computation of the centre-of-mass velocity and the resultant instantaneous moment, the tangential and sideslip velocities

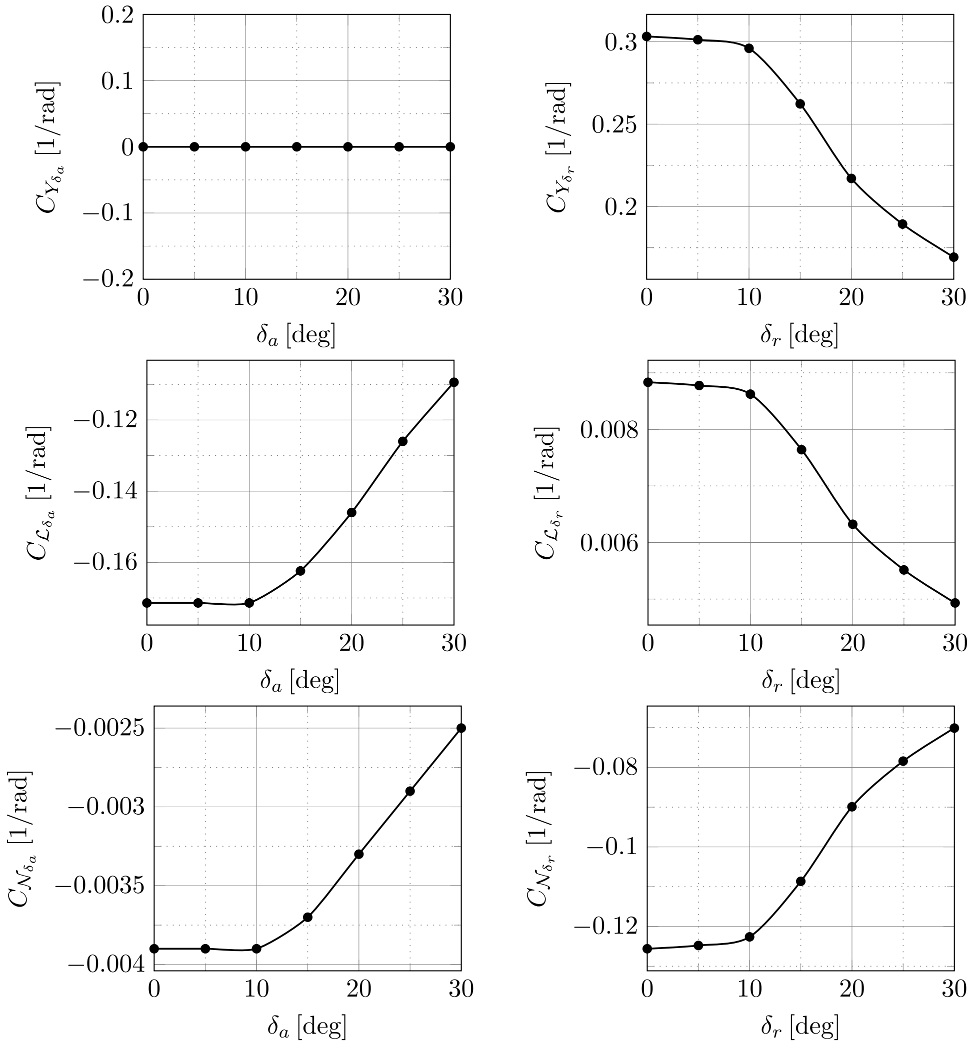

Fig. 8. Computed lateral-directional control derivatives for a simulated C-130J-30 at Mach 0.2.

for each set of wheels can be derived. By subsequently applying well-established friction models from the engineering literature [17,18], the effective friction forces $F_{x,i}$ and $F_{y,i}$, with $i \in \{n, mR, mL\}$, can be determined. These forces, in turn, enable the computation of the reaction moment $\mathcal{N}_{\text{landing gear}}$ as used in (4).

4. Results and discussion

Fig. 6 illustrates the structured input parameters required for the minimum control speed analysis. The methodology employs a systematic Excel-based interface to define aircraft configuration data and facilitate computational workflow management. The computational approach demonstrates remarkable efficiency, enabling a fully nonlinear solution methodology[1] with negligible computational overhead. Complete solutions are generated within seconds across a bank angle range of $\phi = -10$ to $+10°$ with $1°$ increments (Fig. 9), demonstrating that the nonlinear formulation imposes virtually no computational penalty compared to simplified approaches. This efficiency eliminates the traditional trade-off between solution fidelity and computational cost, allowing rigorous nonlinear analysis throughout the conceptual design phase.

[1] https://github.com/GabrieleMorra/Minimum-Control-Speeds-in-Aircraft-Conceptual-Design

Additionally, Figs. 7 and 8 (introduced in Section 4.1) present the full set of stability and control derivatives employed in the analysis. While the implementation supports automation, the focus of this study remains on the methodological development and the resulting estimates of minimum control speeds. Further technical details concerning the input parameters and the lateral-directional equilibrium algorithm are provided in Appendix B.

4.1. Lateral-directional derivatives

The methodology developed in this study relies heavily on the accurate calculation of the aircraft's lateral-directional stability and control derivatives. Particular attention has been devoted to the computation of the coefficients that fill the left-hand side matrices of (1) and (2).

To support the development of a fast and reliable conceptual design methodology suitable for the early design phase, aerodynamic derivatives were estimated using the well-established semi-empirical formulations proposed by Roskam [19]. These methods were further complemented by insights from foundational studies [20] and updated to incorporate more recent developments and experimental validations [21,22].

Figs. 7 and 8 present all the lateral-directional derivatives used in the methodologies developed for the simulated C-130J-30 at Mach number 0.2. The key characteristics of lateral-directional static stability

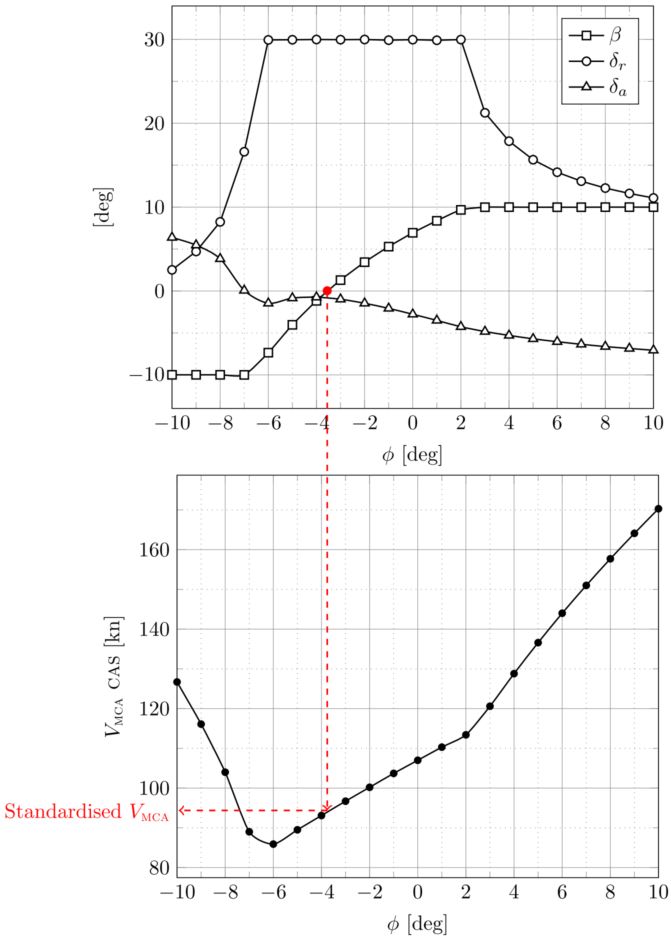

Fig. 9. Multi-axis trim angles and V_{MCA} results for different values of bank ϕ. Aircraft: C-130J-30 with a simulation mass of 45,000 kg.

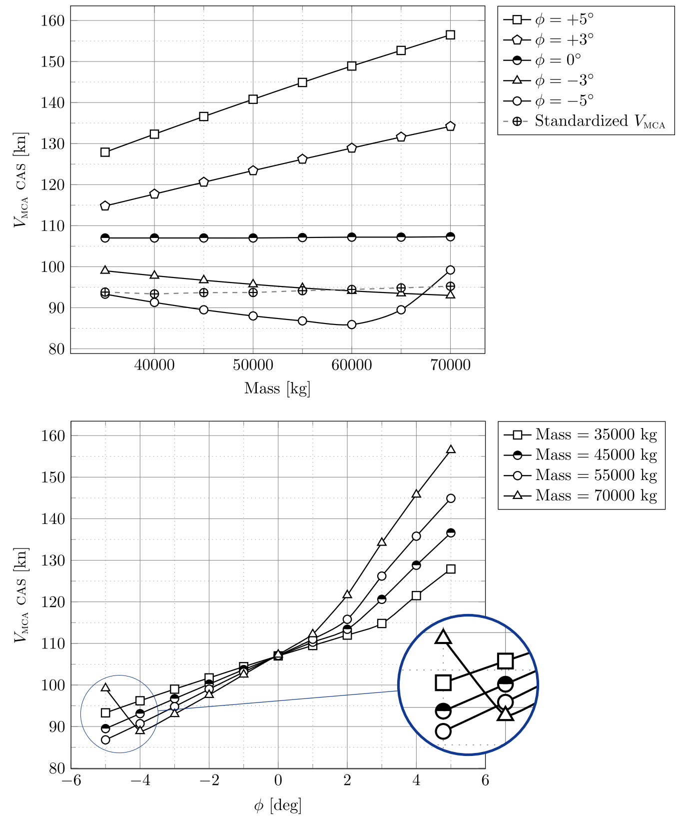

Fig. 10. Effect of bank angle ϕ and flight weight on V_{MCA} for a simulated C-130J-30.

are clearly observable: both $C_{Y_\beta} \cdot \beta$ and $C_{\mathcal{L}_\beta} \cdot \beta$ are negative for positive sideslip angles, indicating the aircraft's inherent stability in response to crosswind disturbances. Notably, the aircraft exhibits a stable yawing tendency, aligning the nose with the wind, as indicated by the positive value of ($C_{\mathcal{N}_\beta}$), which acts to cancel β. The calculation of the derivatives also accounts for the reduction in control effectiveness of $C_{\mathcal{N}_{\delta_r}}$ and $C_{\mathcal{L}_{\delta_a}}$ (see Fig. 8), due to diminished control surface performance at high deflection angles [23]. Additionally, adverse yaw-defined as the aircraft's tendency to yaw in the opposite direction to that intended during an aileron manoeuvre-is incorporated through the derivative $C_{\mathcal{N}_{\delta_a}}$.

4.2. Minimum control speed in air

The results presented are based on the analysis conducted according to the procedure outlined in Fig. 3. The analysis was carried out across a range of bank angles ϕ, from $-10°$ to $10°$, with a step of $1°$, in order to assess the sensitivity of V_{MCA} to lateral trim conditions. Fig. 9 presents the computed values and corresponding trim angles.

The trends reported in the literature are confirmed [12]. All angles comply with the constraints imposed in Table 1. Rudder deflection reaches its maximum for values of $-6° < \phi < 2°$ to achieve lateral-directional trim due to a right critical engine failure, which is considered the critical case. The trend of V_{MCA} is also well captured: the lowest value of the minimum control speed in air occurs at approximately $\phi = -6°$. This indicates that to achieve the lowest possible control speed, the pilot must trim the aircraft with a bank angle away from the failed engine-raising the right wing in this case-resulting in a negative bank angle ϕ.

Important insights also emerge from the analysis of V_{MCA} as a function of aircraft weight. The results shown in Fig. 10 align with the trends reported in the publicly available C-130J Performance Data Manual [24]. Specifically, the minimum control speed increases with increasing weight when the aircraft is banked towards the failed engine-an unfavourable bank angle. Conversely, when the pilot responds appropriately to the OEI condition by banking away from the failed engine, the trend reverses: higher weight becomes advantageous, resulting in a lower minimum control speed. As anticipated, maintaining a wings-level attitude eliminates the effect of weight, since weight does not appear in the lateral-directional trim equations. It is important to note that, as aircraft weight increases, the minimum value of V_{MCA} not only rises but also shifts towards higher values of ϕ. In this context, it is observed that excessive banking-even in the favourable direction, away from the failed engine-can still result in an increase in V_{MCA} (see magnified view in Fig. 10).

The workflow illustrated in Fig. 6 was applied to both the C-130J-30 and the C-130J, yielding results consistent with expectations for this class of aircraft. The C-130J served as a benchmark for validating the methodology, with results compared against data from the Performance Data Manual (PDM) [24], which is publicly available online.

Fig. 11 shows both the carpet plot from the PDM and the results obtained using the proposed methodology. To further evaluate the proposed procedure, another high-wing turboprop aircraft-the ATR 72-500-was simulated, selected due to the public availability of its Flight Crew Operating Manual (FCOM) [25]. For clarity, Tables 2 and 3 present the percentage errors obtained by comparing the V_{MCA} values reported

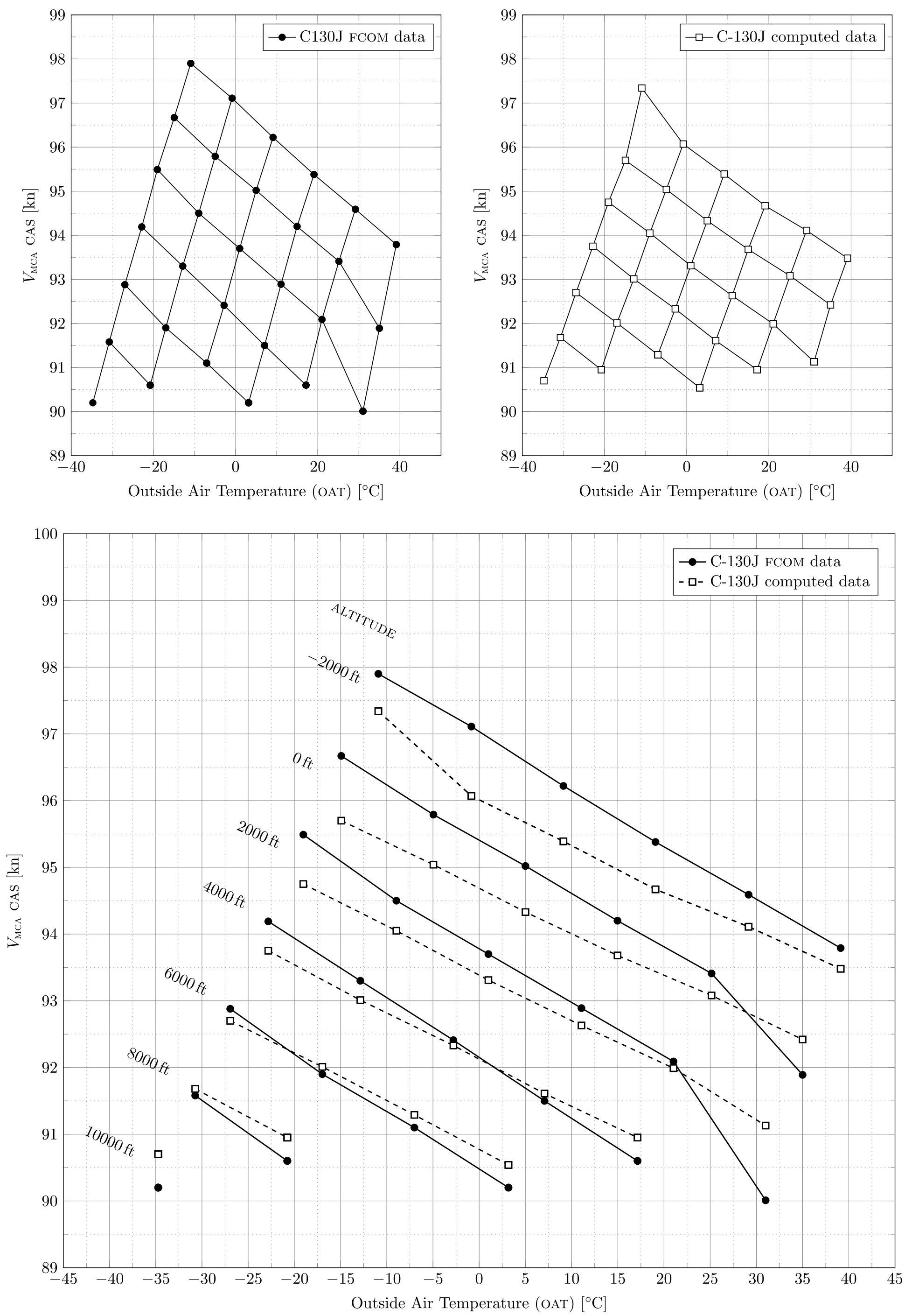

Fig. 11. Reproduction of the C-130J V_{MCA} carpet plot superimposed with calculated values as a function of ΔISA and height.

in the manuals with those estimated using the proposed methodology (Fig. 12).

The validation presented in this study is primarily illustrative and currently limited to two case studies: the C-130J and the ATR 72–500. The availability of public data for such analyses is extremely limited, particularly for more recent aircraft. Nevertheless, the proposed methodology demonstrates promising potential for extension and verification across a broader range of configurations.

A direct comparison between the method presented in this study and the approach proposed by Roskam [7] reveals the percentage improvement in accuracy for estimating V_{MCA}. Fig. 13 illustrates the two methods side by side, across varying altitudes and Outside Air Temperature (OAT) conditions, as applied to the C-130J PDM. In general, the Roskam's method yields higher percentage errors, particularly at higher altitudes. The error associated with the method proposed in this article is predominantly negative, whereas Roskam-s method tends to overestimate. The maximum error observed with the proposed method is 1.24%, while the minimum error recorded using Roskam-s method is 1.14%, clearly demonstrating the advantages of the new approach.

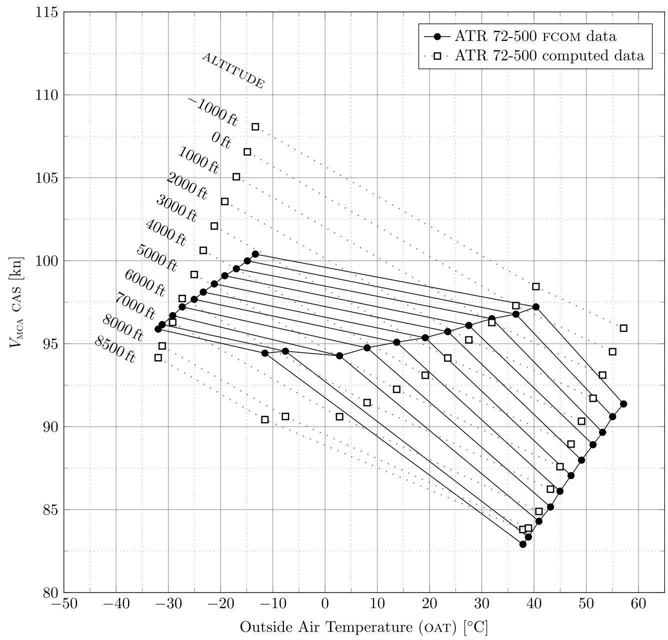

Fig. 12. Reproduction of the ATR 72–500 V_{MCA} carpet plot superimposed with calculated values as a function of ΔISA and height.

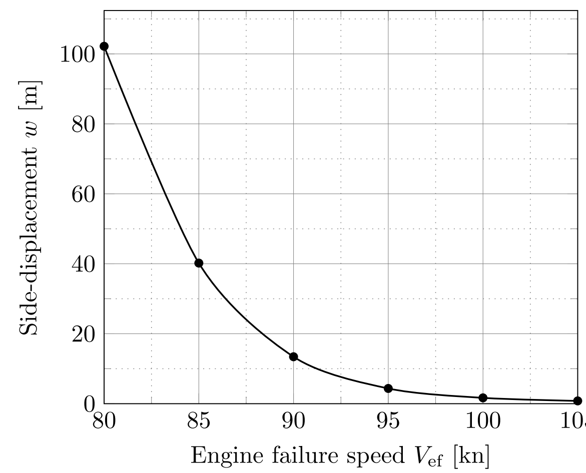

Fig. 14. Trend of side-displacement as a function of the velocity at which the engine failure is simulated. Reference aircraft: C-130J.

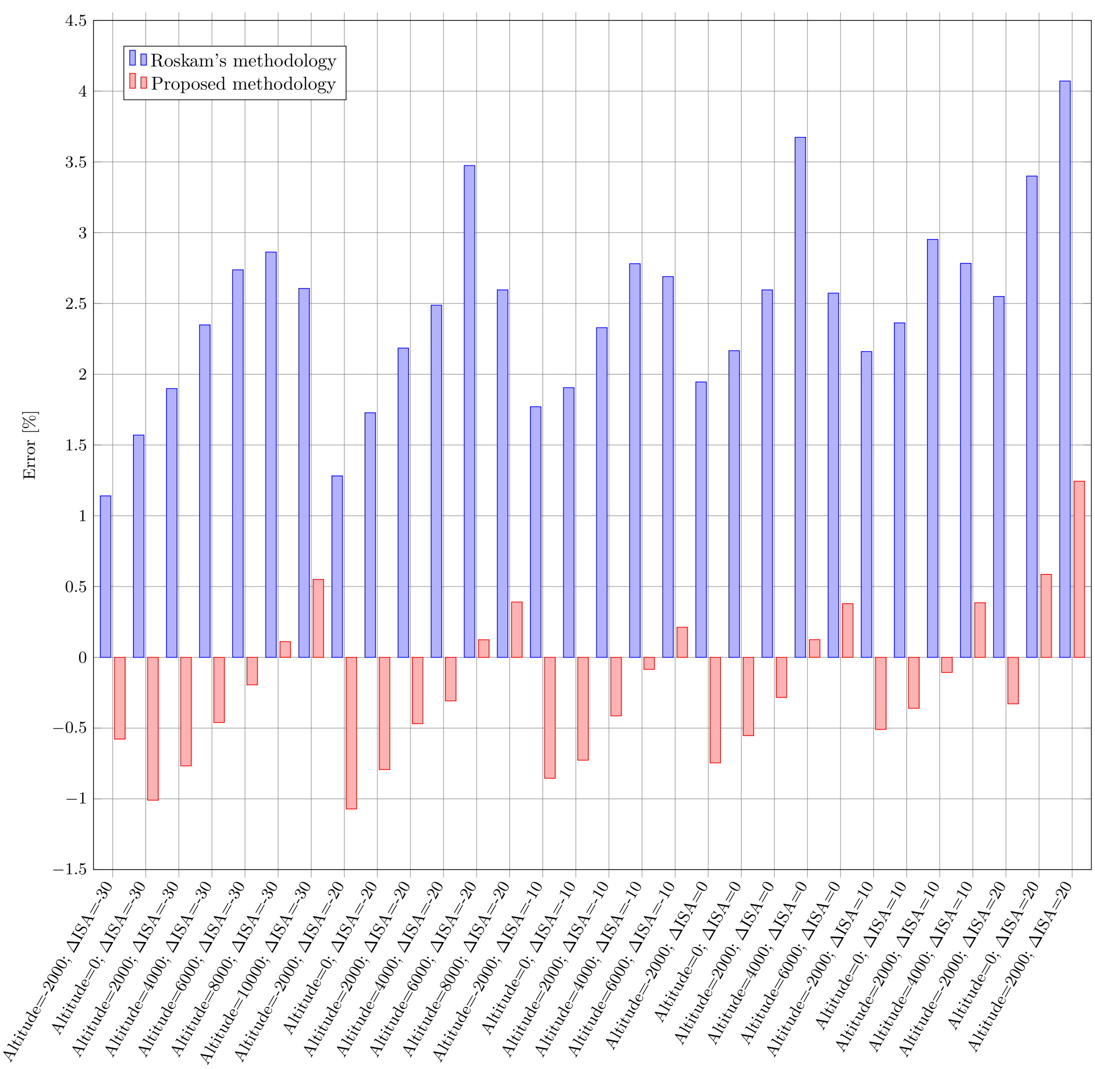

Fig. 13. Comparison of percentage errors in the estimation of V_{MCA} using the proposed methodology and the approach by Roskam, evaluated over a range of pressure altitudes and ΔISA conditions. Reference values are obtained from the C-130J PERFORMANCE DATA MANUAL (PDM).

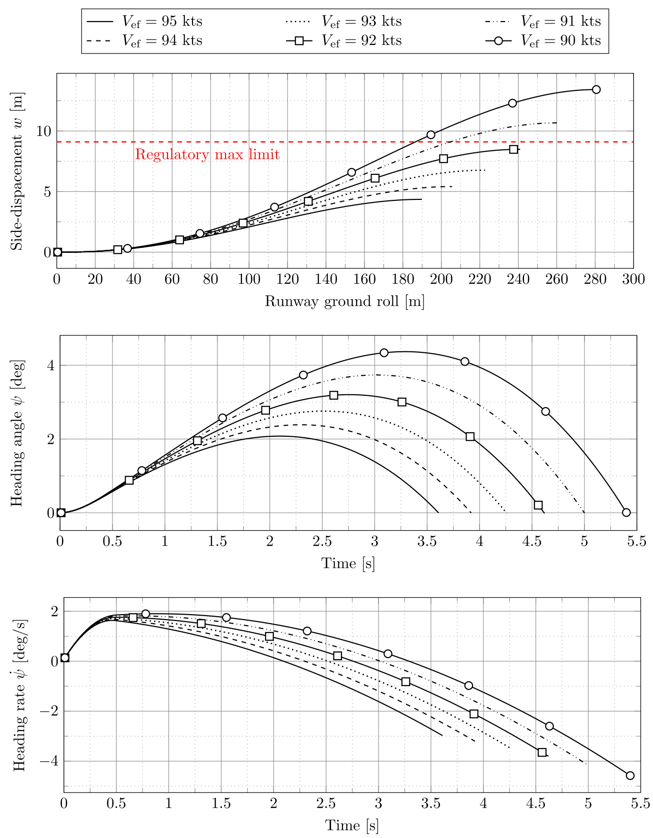

Fig. 15. V_{MCG} simulation manoeuvrers for different engine failure speeds V_{ef} for a modelled C-130J. Simulated trajectories are shown until the aircraft returns to a parallel alignment with the runway. Additionally, variations in heading angle and its rate are presented as a function of time.

A direct comparison between the methodology presented in this study and the classical approach proposed by Roskam [7] highlights the improvements in estimating V_{MCA} accuracy. Fig. 13 shows the percentage errors associated with both methods across varying altitudes and Outside Air Temperature (OAT) conditions, using the C-130J PDM as a reference. Roskam's method generally exhibits larger errors, particularly at higher altitudes, and tends to overestimate V_{MCA}. In contrast, the proposed methodology shows predominantly negative errors, indicating a more consistent behaviour. The maximum absolute error observed with the proposed method is only 1.24%, whereas even the minimum error associated with Roskam-s approach is 1.14%. These results clearly demonstrate the enhanced accuracy and reliability of the non-linear trim-based method introduced in this work.

The comparison was carried out under identical input parameters and flight conditions for both methods, ensuring fully consistent and directly comparable results. To align with regulatory guidance and maintain methodological equivalence, the bank angle ϕ was selected as the value resulting from the lateral-directional trim condition solved in (1) that yields zero sideslip. This choice is consistent with the definition of the standardised V_{MCA}, thereby ensuring that both approaches are evaluated under equivalent constraints. Such alignment allows for a rigorous and meaningful assessment of their relative accuracy.

The implemented methodology enables the rapid generation of reliable results, typically within seconds. These results can be used to inform and refine the vertical tailplane design during the early stages of aircraft development-a particularly critical task for STOL configurations.

Table 2
Error percentage of computed V_{MCA} vs. C-130J FCOM data at various heights and ΔISA.

h [ft]	ΔISA −30 °C Error [%]	ΔISA −20 °C Error [%]	ΔISA −10 °C Error [%]	ΔISA 0 °C Error [%]	ΔISA 10 °C Error [%]	ΔISA 20 °C Error [%]
−2000	−0.58	−0.17	−0.85	−0.75	−0.51	−0.33
0	−0.11	−0.79	−0.73	−0.55	−0.36	0.59
2000	−0.77	−0.47	−0.41	−0.28	−0.11	1.24
4000	−0.46	−0.31	−0.08	0.12	0.39	––
6000	−0.19	0.12	0.21	0.38	—	—
8000	0.11	0.39	—	—	—	—
10,000	0.55	—	—	—	—	—

Table 3
Error percentage of computed V_{MCA} vs. ATR 72–500 FCOM data at various heights and ΔISA.

h [ft]	ΔISA [°C]	Error [%]	ΔISA [°C]	Error [%]	ΔISA [°C]	Error [%]
−1000	−30.00	7.65	23.39	1.26	40.00	5.00
0	−30.00	6.57	21.53	0.53	40.00	4.32
1000	−30.00	5.57	18.91	−0.24	40.00	3.85
2000	−30.00	4.52	16.48	−0.91	40.00	3.15
3000	−30.00	3.54	14.43	−1.66	40.00	2.66
4000	−30.00	2.56	12.09	−2.37	40.00	2.18
5000	−30.00	1.53	8.62	−2.98	40.00	1.72
6000	−30.00	0.52	4.94	−3.48	40.00	1.26
7000	−30.00	−0.42	1.64	−3.90	40.00	0.70
8000	−30.00	−1.34	−6.74	−4.16	40.00	0.25
8500	−30.00	−1.80	−9.68	−4.24	40.00	−0.01

4.3. *Minimum control speed on ground*

The algorithm developed for the calculation of V_{MCG} is initiated at the onset of a simulated engine failure and concludes when the aircraft realigns with the runway direction, as prescribed by EASA CS 25.149(e) [10]. Multiple manoeuvres were simulated at varying engine failure speeds V_{ef}, as illustrated in Figs. 14 and 15. Notably, even small variations in V_{ef} result in significant changes in lateral displacement. This sensitivity arises because the simulations are conducted at speeds near the lift-off threshold, which corresponds to the maximum ground speed reached during the takeoff roll. Consequently, although the aircraft exhibits only modest deviations in heading angle ψ-typically within a few degrees-the elevated ground speed substantially amplifies the lateral displacement.

The results obtained are consistent with the literature [26,27], demonstrating that the developed calculation procedure meets the expectations. To further investigate the quality of the results, Fig. 16 compares the computed carpet plot of V_{MCG} with the corresponding plot from the PDM. Fig. 17 presents the resultant percentage errors.

These calculations are valuable for meeting takeoff requirements on narrow runways where lateral deviation must be minimised. An approach for estimating minimum control speed on the ground during the early design stages enables designers to evaluate the aircraft-s operational envelope effectively. Moreover, the methodology can be readily adapted to accommodate different runway surfaces (asphalt, unprepared, etc.) and potential contaminants. As such, it represents an important tool in the design of tactical military aircraft.

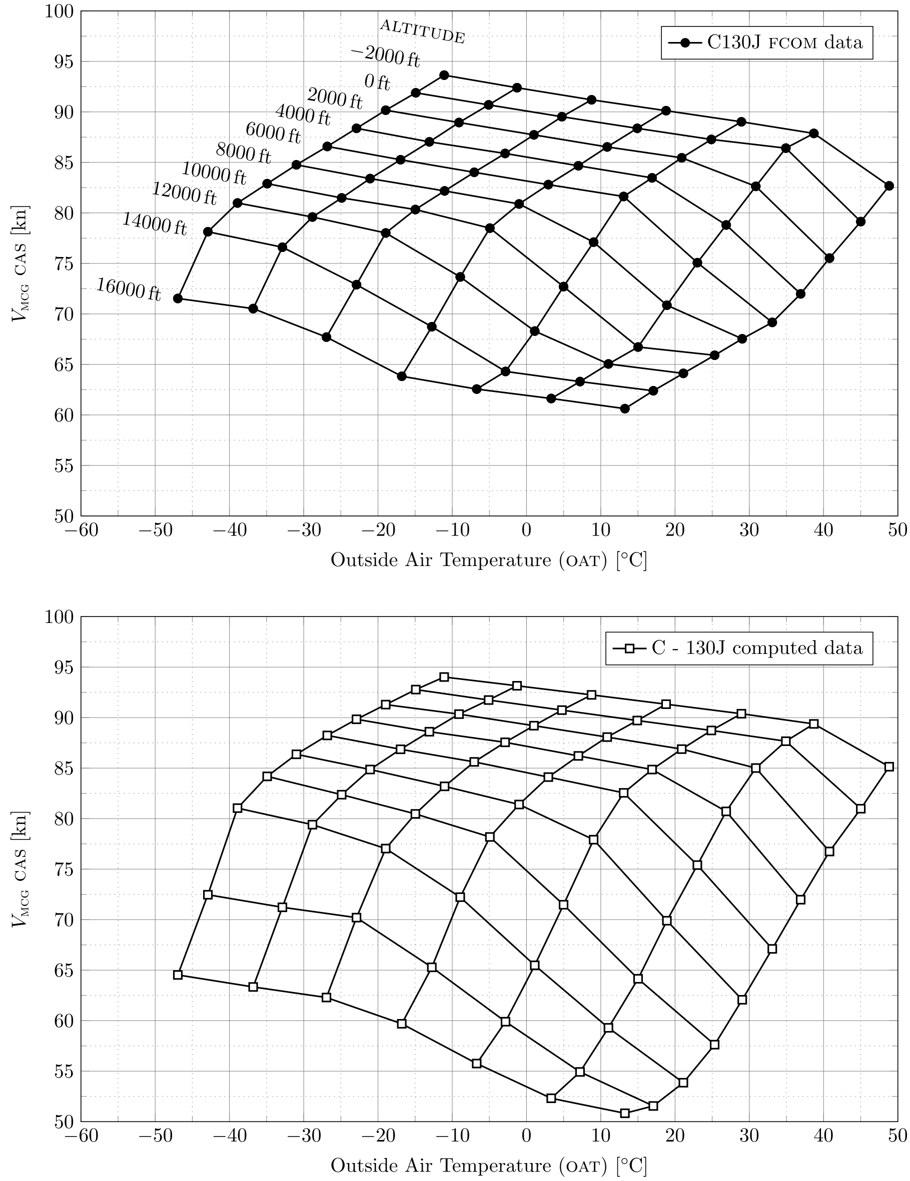

Fig. 16. Reproduction of the computed and PDM C-130J V_{MCG} carpet plots.

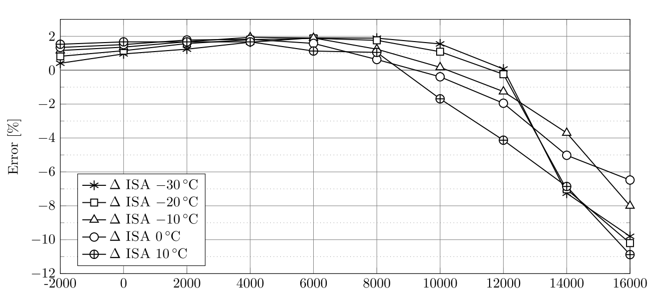

Fig. 17. Error percentage of computed V_{MCG} vs. C-130J PDM data at various heights and ΔISA.

5. Conclusions

Current aircraft design practices often rely on simplified assumptions that do not fully capture the complexity of modern aircraft configurations, particularly regarding the estimation of critical flight speeds. The increasing sophistication of contemporary aircraft designs, coupled with stringent safety requirements, necessitates more accurate and comprehensive methodologies for determining minimum control speeds during the conceptual design phase. Early-stage design decisions significantly influence subsequent development costs, making the availability of reliable estimation tools essential for manufacturers to make informed design choices and optimize aircraft performance characteristics.

The methodology proposed in this work addresses current limitations in the estimation of minimum control speeds, providing engineers with a practical tool during the conceptual design phase. Notably, it requires only a limited set of input parameters, making it well-suited for integration into early stages of design loops-even when detailed aircraft data are not yet available.

This study introduces a comprehensive methodology for evaluating minimum control speeds both in the air (V_{MCA}) and on the ground (V_{MCG}) during the conceptual design of large aircraft. The proposed framework incorporates the solution of lateral-directional trim equations and a time-domain simulation that accounts for landing gear-runway interaction effects-factors often oversimplified or neglected in early-stage design tools. By simulating engine-out manoeuvres and integrating these dynamic effects, the methodology offers a more accurate representation of the underlying physics.

The approach also incorporates the constraints imposed by airworthiness regulations. By replicating certification-relevant manoeuvres, the methodology supports an early-stage consistency check with the requirements specified in CS and FAR, thereby contributing to a design process more likely to comply with safety requirements and regulations.

The methodology has demonstrated its suitability for supporting conceptual design activities, with computed V_{MCA} values showing minimal deviation from reference data and significant improvements over conventional simplified approaches. Validation against the C-130J PDM indicates errors generally below 1%, confirming both the enhanced accuracy and practical applicability of the methodology.

Similarly, the V_{MCG} results exhibit strong agreement with reference data, further confirming the reliability of the proposed methodology. This consistency allows for an early assessment of whether a given aircraft configuration complies with runway width constraints, thereby offering a practical and valuable support tool for conceptual design.

The results obtained, along with their comparison to data presented on the AFMs demonstrate a clear correspondence. However, the analysis was limited to two aircraft for which publicly available data and technical documentation were accessible. This constraint highlights the general lack of high-fidelity performance information in the public domain, particularly for modern configurations. Future work may address this limitation by extending the validation to a broader database of aircraft, including both contemporary and legacy designs.

CRediT authorship contribution statement

Gabriele Morra: Writing – review & editing, Writing - original draft, Visualization, Validation, Software, Methodology, Investigation, Data curation, Conceptualization; **Claudio Mirabella:** Writing – review & editing, Writing - original draft, Visualization, Investigation; **Fabrizio Nicolosi:** Writing – review & editing, Supervision; **Pierluigi Della Vecchia:** Writing – review & editing.

Data availability

Data will be made available on request

Declaration of competing interest

The authors declare that they have no known competing financial interests or personal relationships that could have appeared to influence the work reported in this paper.

Appendix A. Regulatory framework

This appendix provides a more detailed overview of the regulatory provisions and testing procedures required to establish minimum control speeds for aircraft certification, as defined by EASA CS-25 and FAA FAR-25.

The Acceptable Means of Compliance (AMC) allow for the use of both static and dynamic methods to determine the minimum control speed. In static testing, the aircraft is initially placed in a trimmed flight condition with asymmetric thrust, which is then progressively reduced until directional control can no longer be maintained. A limited number of dynamic tests-typically involving the sudden failure of the critical engine-are conducted to validate the static results. According to regulatory guidance, loss of control must be indicated by either a clear divergence from the intended flight path or a marked degradation in directional stability.

The definition of Minimum Control Speed (V_{MC}) given by EASA CS - 25 is the following:

> **CS 25.149.(b)** V_{MC} is the *calibrated airspeed*, at which, when the critical engine is suddenly made inoperative, it is possible to maintain control of the aeroplane with that engine still inoperative and maintain straight flight with an angle of bank of not more than 5°.

The Minimum Control Speed is closely related to the *Reference Stall Speed* V_{SR}; specifically, it must not exceed $1.13 \cdot V_{SR}$ when the aircraft has the following configuration:

1. Maximum available takeoff power or thrust on the engines.
2. The most unfavourable centre of gravity.
3. The aeroplane is in a trimmed configuration for takeoff.
4. The maximum sea - level takeoff weight (or any lesser weight necessary to show V_{MC}).
5. The aeroplane in the most critical takeoff configuration existing along the flight path after the aeroplane becomes airborne, except with the landing gear retracted.
6. The aeroplane airborne and the ground effect is negligible.
7. If applicable, the propeller of the inoperative engine:
   (a) Windmilling.
   (b) In the most probable position for the specific design of the propeller control.
   (c) Feathered, if the aeroplane has an automatic feathering device acceptable for showing compliance with the climb requirements of CS 25.121.

Another limitation concerns the maximum allowable rudder control force, which must not exceed 667N. Furthermore, maintaining controlled flight should not require any reduction in engine power or thrust.

This limitation also applies during the determination of the V_{MCG}, which is the minimum control (calibrated) speed on the ground during the takeoff run at which it is still possible to maintain directional control of the aircraft using the rudder input alone, without relying on nose - wheel steering. Lateral control may be used only to the extent necessary to keep the wings level. The aircraft must remain controllable using average piloting skill when the critical engine is suddenly rendered inoperative. During this test, the aircraft must not deviate laterally by more than 9.1m (30ft) from the runway centreline. Fig. A.18 shows a sketch of this scenario. The recovery manoeuvre must not result in a hazardous aircraft attitude or require abnormal piloting skill, alertness, or strength to prevent a heading change exceeding 20°. To establish the V_{MCG} adequately, the following conditions must be met:

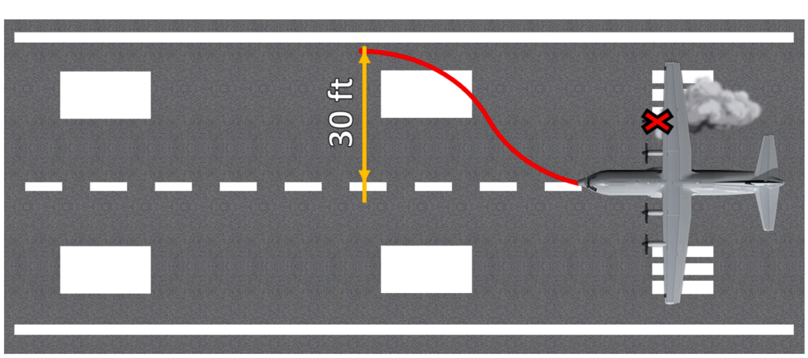

Fig. A.18. A sketchy representation of the test - case scenario depicted in EASA CS 25.149.(e) and FAA CFR 25.149.(e) (*Minimum Control Speed*).

1. The aeroplane in each takeoff configuration or, at the option of the applicant, in the most critical takeoff configuration.
2. Maximum available takeoff power/thrust on the operating engine/s.
3. The most unfavourable centre of gravity.
4. The aeroplane is in a trimmed takeoff configuration.
5. The most unfavourable weight in the range of takeoff weights.

Similar requirements apply during landing operations. EASA designates the minimum control (calibrated) speed during approach or landing-with all engines operating when the critical engine is suddenly rendered inoperative-as V_{MCL}. At this speed, the aircraft must remain controllable with the inoperative engine and be capable of maintaining straight flight with a bank angle not exceeding 5°.

Appendix B. Algorithms input parameters

(Tables B.4, B.5, B.6.)

Table B.4
Main geometrical and aerodynamic input parameters of the ATR 72–500 and the Lockheed Martin C-130J.

	PARAMETER	ATR 72–500	C-130J	
WING	Surface	61.0	162.0	m^2
	Span	27.05	40.41	m
	Dihedral	0.42	1.85	deg
	Height	−1.585	−2.419	m
	Average sweep of the equivalent wing	3.6	1.0	deg
	Aileron maximum deflection	20.0	20.0	deg
	Taper ratio	0.579	0.520	
	Tip x position	11.645	11.5	m
	Geometric twist	0.0	3.0	deg
	Thickness/chord ratio at aileron station	8.0	8.0	%
	Aileron chord fraction	0.2	0.25	
	Airfoil lift curve slope at aileron station	6.0	6.0	rad^{-1}
	Aileron inner position/semi span	75.0	70.0	%
	Aileron outer position/semi span	98.0	98.0	%
FUSELAGE	Reference diameter	3.311	4.654	m
	Diameter at vertical tail quarter chord	1.835	3.000	m
	Length	27.07	29.79	m
	Section area S_0 [19, p. 385]	5.922	11.506	m
	Volume	135.7	307.0	m^3
HORIZ. TAIL	Surface	11.56	50.63	m^3
	Span	7.31	16.05	m
	Sweep half chord	4.726	3.437	deg
	Height w.r.t. waterline	4.751	1.68	m
	Dynamic pressure ratio η	1.0	0.85	
VERT. TAIL	Rudder chord fraction	0.25	0.25	
	Span	4.468	7.041	m
	Sweep quarter chord	38.47	17.0	deg
	Chord root	4.77	6.3	m
	Chord tip	1.91	1.8	m
	Aerodynamic centre height w.r.t. waterline	1.461	3.057	m
	Aerodynamic centre distance from centre of mass	10.826	16.500	m
	Rudder maximum deflection	30.0	30.0	deg
	Rudder/vertical span	75	100	%
	Thickness/chord ratio at rudder station	8	8	%

Table B.5
Miscellaneous input parameters for V_{MCA} analysis of the ATR 72–500 and V_{MCA} & V_{MCG} analysis of the Lockheed Martin C-130J.

	PARAMETER	ATR 72–500	C-130J	
V_{MCA}	$C_{L,\,max}$ Takeoff	2.1	2.1	
	Number of engine	2	4	
	Nacelle reference diameter	1.063	1.213	m
	Max static thrust	32,721	54,000	N
	Worst case scenario engine failure arm length	4.05	10.17	m
V_{MCG}	$C_{L,\,max}$ Ground	—	0.9	
	$\overline{R_z}$ [p. 198, 199, 200]	—	0.49	
	Rudder angular velocity	—	60	deg/s
	Operating empty mass	—	35,000	kg
	$C_{D,0}$ Takeoff	—	0.075	
	Oswald efficiency factor	—	0.8	
	Longitudinal position of the main landing gear w.r.t. centre of gravity x_{main}	—	1.0	m
	Lateral position of the main landing gear w.r.t. centre of gravity y_{main}	—	11.0	m
	Lateral position of the nose landing gear w.r.t. centre of gravity x_{nose}	—	2.67	m

Table B.6
Solver settings input parameters for mass and weight analyses for the Lockheed Martin C-130J.

	PARAMETER	C-130J	
SOLVER SETTINGS	Mach number M	0.3	
	Max side-displacement (for V_{MCG})	9.144	m
	Mass start	35,000	kg
	Mass end	70,000	kg
	Mass step	5000	kg
	Initial bank angle ϕ_{start}	−10	deg
	Initial bank angle ϕ_{start}	10	deg
	Bank angle step $\Delta\phi$	1	deg
	Speed increment step size ΔV	0.1	kn
	Nonlinear solver tolerance	10^{-15}	

Appendix C. Supplementary data

This section presents all the data produced by the C# routines, which are also intended to support reproducibility of the work. These data are the outputs of the V_{MCA} and V_{MCG} direct calculations, as shown by diagrams and graphs in this article. Table C.7 provides data about the V_{MCG}; Tables C.8, C.9, and C.10 illustrate lateral-directional derivatives concerning the sideslip angle beta; Tables C.11 and C.12 show lateral-directional control derivatives. Table C.13 shows results from the solution of the nonlinear, indeterminate system of equations. Finally, C.14 is a lookup table which collects V_{MCA} data as a function of the aircraft's bank angle phi and weight.

V_{MCG} data of Fig. 15 are available at the following GitHub repository: https://github.com/GabrieleMorra/Vmcg-simulation-maneuvers-data. Table C.15 shows all data of how V_{MCG} varies with several engine failure speeds.

Table C.7
Numerical data represented in Fig. 4 concerning the yawing moment due to critical engine failure $\mathcal{N}_T$ and rudder control moment $\mathcal{N}_{\delta_r}$ for a simulated C-130J. $\mathcal{N}_T$ and $\mathcal{N}_{\delta_r}$ represent the magnitudes of the associated vectors.

V [kn]	$\mathcal{N}_T$ [Nm]	$\mathcal{N}_{\delta_r}$ [Nm]
0	544,034	0
10	540,912	5028
20	536,579	20,110
30	530,772	45,242
40	530,772	80,419
50	522,697	125,631
60	511,358	180,867
70	497,740	246,113
80	482,007	321,351
90	464,555	406,559
100	447,053	501,712
110	429,733	606,780
120	412,770	721730
130	396,172	846,522
140	380,266	981,109
150	364,869	1,125,439
160	349,777	1,279,452

Table C.8
Numerical data represented in Fig. 7 concerning yawing lateral-directional stability derivatives for a simulated C-130J.

β [°]	$C_{\mathcal{N}_{\text{Wing}}}$	$C_{\mathcal{N}_{\text{Fuselage}}}$	$C_{\mathcal{N}_{\text{Vertical}}}$	
−10	0.000079	0.010977	−0.028139	−0.017080
−7	0.000053	0.007318	−0.018759	−0.011390
−3	0.000026	0.003659	−0.009380	−0.005690
0	0.000000	0.000000	0.000000	0.000000
3	−0.000026	−0.003659	0.009380	0.005690
7	−0.000053	−0.007318	0.018759	0.011390
10	−0.000079	−0.010977	0.028139	0.017080

Table C.9
Numerical data represented in Fig. 7 concerning roll lateral-directional stability derivatives for a simulated C-130J.

β [°]	$C_{\mathcal{L}_{\text{Wing-Body}}}$	$C_{\mathcal{L}_{\text{Vertical}}}$	$C_{\mathcal{L}_{\text{Horizontal}}}$	$C_{\mathcal{L}}$
−10	0.013069	0.004982	0.000000	0.018052
−7	0.008713	0.003322	0.000000	0.012034
−3	0.004356	0.001661	0.000000	0.006017
0	0.000000	0.000000	0.000000	0.000000
3	−0.004356	−0.001661	0.000000	−0.006017
7	−0.008713	−0.003322	0.000000	−0.012034
10	−0.013069	−0.004982	0.000000	−0.018052

Table C.10
Numerical data represented in Fig. 7 concerning side-force lateral-directional stability derivatives for a simulated C-130J.

β [°]	$C_{Y_{\text{Wing-Body}}}$	$C_{Y_{\text{Vertical}}}$	$C_{Y_{\text{Horizontal}}}$	C_Y
10	0.001850	0.097171	0.067928	0.166950
−7	0.001233	0.064781	0.045285	0.111300
−3	0.000617	0.032390	0.022643	0.055650
0	0.000000	0.000000	0.000000	0.000000
3	−0.000617	−0.032390	−0.022643	−0.055650
7	−0.001233	−0.064781	−0.045285	−0.111300
10	−0.001850	−0.097171	−0.067928	−0.166950

Table C.11
Numerical data represented in Fig. 8 concerning lateral-directional control derivatives with respect to δ_a for a simulated C-130J.

δ_a [°]	$C_{Y_{\delta_a}}$	$C_{\mathcal{L}_{\delta_a}}$	$C_{\mathcal{N}_{\delta_a}}$
0	0.000000	−0.171400	−0.003900
5	0.000000	−0.171400	−0.003900
10	0.000000	−0.171400	−0.003900
15	0.000000	−0.162400	−0.003700
20	0.000000	−0.146000	−0.003300
25	0.000000	−0.126000	−0.002900
30	0.000000	−0.109400	−0.002500

Table C.12
Numerical data represented in Fig. 8 concerning lateral-directional control derivatives with respect to δ_r for a simulated C-130J.

δ_a [°]	$C_{Y_{\delta_a}}$	$C_{\mathcal{L}_{\delta_a}}$	$C_{\mathcal{N}_{\delta_a}}$
0	0.303211	0.008833	−0.125602
5	0.301239	0.008776	−0.124786
10	0.296013	0.008623	−0.122620
15	0.262289	0.007641	−0.108651
20	0.217038	0.006323	−0.089906
25	0.189332	0.005516	−0.078429
30	0.169274	0.004931	−0.070120

Table C.13
Numerical data represented in Fig. 9 concerning multi-axis trim angles and V_{MCA} with different bank angles ϕ for a simulated C-130J. The simulation mass is 45,000 kg.

ϕ [°]	β [°]	δ_r [°]	δ_a [°]	V_{MCA} [kn]
−10	−9.99	2.52	6.38	126.7
−9	−9.99	4.71	5.47	116.1
−8	−9.99	8.24	3.84	104.0
−7	−10.00	16.60	0.07	89.0
−6	−7.35	29.93	−1.46	85.9
−5	−4.03	29.95	−0.84	89.5
−4	−1.17	29.98	−0.74	93.1
−3	1.30	29.96	−0.98	96.7
−2	3.44	29.98	−1.46	100.2
−1	5.29	29.90	−2.07	103.7
0	6.94	29.96	−2.77	107.0
1	8.37	29.89	−3.50	110.3
2	9.67	29.97	−4.26	113.4
3	9.99	21.24	−4.83	120.6
4	10.00	17.86	−5.29	128.8
5	9.99	15.65	−5.70	136.6
6	9.99	14.16	−6.04	144.0
7	9.99	13.09	−6.35	151.0
8	10.00	12.27	−6.62	157.7
9	10.00	11.63	−6.85	164.1
10	10.00	11.09	−7.06	170.3

Table C.14
Lookup table represented in Fig. 10. Change in V_{MCA} with aircraft bank angle ϕ and flight mass for a simulated C-130J.

	ϕ [°]										
Mass [kg]	−5	−4	−3	−2	−1	0	1	2	3	4	5
35,000	93.3	96.2	99	101.7	104.4	107	109.5	112	114.8	121.5	127.9
40,000	91.3	94.6	97.8	101	104	107	109.9	112.7	117.7	125.2	132.3
45,000	89.5	93.1	96.7	100.2	103.7	107	110.3	113.4	120.6	128.8	136.6
50,000	88	91.8	95.7	99.6	103.4	107	110.6	114.1	123.4	132.4	140.8
55,000	86.8	90.7	94.8	99	103.1	107.1	111	115.8	126.2	135.8	144.9
60,000	85.9	89.9	94.1	98.4	102.8	107.2	111.4	117.8	128.9	139.2	148.9
65,000	89.5	89.2	93.5	98	102.6	107.2	111.8	119.7	131.6	142.5	152.7
70,000	99.2	88.9	93	97.6	102.5	107.3	112.2	121.6	134.2	145.8	156.5

Table C.15
Numerical data represented in Fig. 14 concerning trend of side-displacement as a function of the velocity at which the engine failure happens for a simulated C-130J.

w [M]	V_{ef} [ms^{-1}]
0.80	105
1.67	100
4.36	95
13.42	90
40. 20	85
102.18	80

References

[1] A.T.S. Bureau, Australian transport safety bureau, loss of control - embraer S.A. EMB-120ER Brasilia, VH-ANB, darwin airport, Northern Territory, on 22 March, (2010). Technical Publications (accessed on September 23, 2024), https://www.atsb.gov.au/publications/investigation_reports/2010/aair/ao-2010-019.

[2] M. Lacagnina, Fatal V1 cut, AeroSafety World 7 (2012) 24–28.

[3] H. Horlings, Airplane control and analysis of accidents after engine failures, (2010). AvioConsult Available online: https://avioconsult.com/downloads/Airplane%20Control%20and%20Analysis%20of%20Accidents%20after%20Engine%20Failure.pdf (accessed on September 23, 2024).

[4] S. Corcione, M. Mandorino, V. Cusati, Beyond conventional: an integrated aerostructural optimization approach for innovative tailplane configurations, Aerosp. Sci. Technol. 150 (2024) 109242.

[5] M.H. Sadraey, Aircraft Design: A Systems Engineering Approach, John Wiley & Sons, 2024.

[6] E. Torenbeek, Synthesis of Subsonic Airplane Design: An Introduction to the Preliminary Design of Subsonic General Aviation and Transport Aircraft, with Emphasis on Layout, Aerodynamic Design, Propulsion and Performance, Springer Science & Business Media, 2013.

[7] J. Roskam, Airplane Design VII: Determination of Stability, Control and Performance Characteristics: FAR and Military Requirements, 7, DARcorporation, 1985.

[8] E.M. Hadder, T.T. Takahashi, Minimum control speed estimation for conceptual design, in: 17th AIAA Aviation Technology, Integration, and Operations Conference, 2017, p. 3764.

[9] A.D. Marco, V. Trifari, F. Nicolosi, M. Ruocco, A simulation-based performance analysis tool for aircraft design workflows, Aerospace 7 (11) (2020) 155.

[10] EASA, Certification specifications for large aeroplanes, Certification Specifications Amendment 27 (27) (2023).

[11] FAA, Title 14 CFR, part 25, airworthiness standard: transport category aircraft, Federal Aviation Rules Amendment 64 (2024).

[12] H. Horlings, Control and performance during asymmetrical powered flight, Change 2016 (2012) 05-04.

[13] H.S. Gill, (2023). Not Applicable https://github.com/profhsgill/HSG.Numerics.

[14] J.J. Moré, D.C. Sorensen, K.E. Hillstrom, B.S. Garbow, The MINPACK project, Sources Dev. Math. Softw. 25 (1984) 88–111.

[15] C. Lelaie, Estimating the air minimum control speed, Saf. First (2011) 1–5. Accessed on August 23, 2024, https://safetyfirst.airbus.com/safety-first-magazine/issue-11-january-2011/.

[16] J. Roskam, Airplane Design V: Component Weight Estimation, 5, DARcorporation, 1985.

[17] E.S.D. Unit, Frictional and Retarding Forces on Aircraft Tyres. Part II: Estimation of Braking Force, Technical Report ESDU 71026, Engineering Sciences Data Unit (ESDU), London, UK, 1971.

[18] T.J. Yager, J.L. McCarty, Friction Characteristics of Three 30 x 11.5–14.5, Type VIII, Aircraft Tires With Various Tread Groove Patterns and Rubber Compounds, Technical Paper, NASA, 1977.

[19] J. Roskam, Airplane Design VI: Preliminary Calculation of Aerodynamic, Thrust and Power Characteristics, 6, DARcorporation, 1985.

[20] C.D. Perkins, Airplane Performance, Stability and Control, John Wiley & Sons, 1949.

[21] F. Nicolosi, P. Della Vecchia, D. Ciliberti, An investigation on vertical tailplane contribution to aircraft sideforce, Aerosp. Sci. Technol. 28 (1) (2013) 401–416.

[22] F. Nicolosi, D. Ciliberti, P. Della Vecchia, S. Corcione, Experimental analysis of aircraft directional control effectiveness, Aerosp. Sci. Technol. 106 (2020) 106099.

[23] C. work, A comprehensive review of vertical tail design, in: 6th Symposium on Collaboration in Aircraft Design Warsaw, Poland, 2016, p. All. https://doi.org/10.13140/RG.2.2.12606.69448

[24] Performance Data Manual for Aeronautica Militare Italiana Series C-130J and KC-130J Airplanes Model 382U Airplanes, Lockheed Martin Aeronautics Company, 2006. Available: https://www.docdroid.com/pDQh0cn/italian-c-130j-performance-manual-pdf [Accessed: 30-Sep-2024].

[25] Flight Crew Operating Manual: ATR 72–500, Avions de Transport Régional, 1994. Available online: https://aviation-is.better-than.tv/atr72fcom.pdf (accessed on September 23, 2024).

[26] H. Chengtao, W. Lixin, J. Zhongren, A method to calculate the aircraft ground minimum control speed based on mathematical simulation, Procedia Eng. 17 (2011) 24–38.

[27] E.-J. A.M. Huijbrechts, H.J. Koolstra, J.A. Mulder, Using V MCG-Limited V 1, controllability issues on contaminated runways and in crosswind, J. Aircr. 56 (4) (2019) 1342–1352.